Support Vector Machine for Prediction of the Electronic Factors of a Schottky Configuration Interlaid with Pure PVC and Doped by Sm2O3 Nanoparticles

Article *in* Advanced Electronic Materials · October 2024

DOI: 10.1002/aelm.202400624

CITATIONS
2

READS
76

3 authors:

Yashar Azizian
University of Mohaghegh Ardabili
189 PUBLICATIONS **4,220** CITATIONS
SEE PROFILE

Yosef Badali
Istanbul Ticaret University
36 PUBLICATIONS **567** CITATIONS
SEE PROFILE

Ali Barkhordari
33 PUBLICATIONS **447** CITATIONS
SEE PROFILE

ADVANCED ELECTRONIC MATERIALS Open Access
www.advelectronicmat.de

Support Vector Machine for Prediction of the Electronic Factors of a Schottky Configuration Interlaid with Pure PVC and Doped by Sm_2O_3 Nanoparticles

Yashar Azizian-Kalandaragh, Ali Barkhordari,* and Yosef Badali*

This work uses the Support Vector Machine (SVM) to predict the main electronic variables of metal-semiconductor (MS) and metal-nanocomposite-semiconductor (MPS) configurations, i.e., leak current (I_0), the height of the potential barrier (Φ_{B0}), ideality coefficient (n), series/shunt resistances (R_s/R_{sh}), rectification ratio (RR), and surface/interface states density (N_{ss}), along with current conduction/transport mechanisms occurred into them at the reverse/forward biases by analyzing the I–V measurements. The polyvinyl chloride (PVC) and samarium oxide (Sm_2O_3) nanoparticles are combined to form the two interfacial layers. To analyze the I–V characteristics and train the SVM, the thermionic emission theorem is used. By contrasting the predicted and experimental results, the predictive ability of the SVM approach for predicting the electronic specifications of the fabricated structures and their current conduction/transport processes has been evaluated to investigate the effectiveness of the SVM. There is strong agreement between the experimental data and the SVM predictions of the fundamental electronic characterizations of the MS and MPS structures and the current conduction processes in them at the forward/reverse biases. Additionally, the results demonstrate that the RR value of the MS configuration increases 4 and 53 times if the pure PVC and PVC:Sm_2O_3 composite interlayers are employed.

1. Introduction

Due to its capacity for either rectification or non-rectification behavior, Schottky structures, or MS-type structures/contacts, are formed once a metal joins the semiconductor. These structures are significant electrical devices in solid-state physics. The primary factor allowing electrical current to flow in a single direction is the potential established at the MS contact interface.[1–3] However, using other preparation techniques, such as thermal or anodic oxide, the formed insulator-layer between the semiconductor and the metal is unable to fully passivate the active dangling bonds on the semiconductor's surface.[4–9] As a result, a number of researches have recently been published that describe devices made employing metallic/metallic-oxide elements doped interfacial organic or polymer layer in contrast to earlier techniques.[10,11]

Rocha et al. explored the electrical and material features of plasma-enhanced atomic layer deposited (PE-ALD) AlON on dry-etched n-type GaN substrates with nitrogen concentrations from 1.5% to 7.1%. They observed that higher nitrogen concentrations led to increased flat-band voltage (V_{FB}) and hysteresis, with V_{FB} correlating to nitrogen levels and hysteresis linked to impurities like hydroxyl and carbon compounds. The study also assessed various post-deposition annealing (PDA) temperatures between 400 and 800 °C, noting stable AlON layers and interfaces with

Y. Azizian-Kalandaragh
Department of Photonics
Faculty of Applied Sciences
Gazi University
Ankara 06500, Turkey
E-mail: yasharazizian@gazi.edu.tr
Y. Azizian-Kalandaragh
Photonics Application and Research Center
Gazi University
Ankara 06500, Turkey
The ORCID identification number(s) for the author(s) of this article can be found under https://doi.org/10.1002/aelm.202400624

DOI: 10.1002/aelm.202400624

Y. Azizian-Kalandaragh
Department of Physics
University of Mohaghegh Ardabili
Ardabil 56131, Iran
A. Barkhordari
Faculty of Physics
Shahid Bahonar University of Kerman
Kerman 76131, Iran
E-mail: alibarkhordari20@phy.uk.ac.ir
Y. Badali
Department of Computer Engineering
Istanbul Ticaret University
Istanbul 34445, Turkey

minor gallium oxide growth and gallium diffusion. As PDA temperature rose, both V_{FB} and the interface state density (D_{it}) diminished significantly, especially at 150 °C. These findings suggest a promising direction for improving the reliability and stability of normally-OFF GaN-based MOS-channel high electron mobility transistors.[12]

The performance of the MS structure is thought to be improved by using a high-dielectric polymer or composite in terms of a rise in the barrier height (BH) formed at the interface amidst the semiconductor and metal layers and rectification rate (RR), a reduction in the surface states density (N_{ss}) created at the interface of interlayer and semiconductor and series resistance (R_s).[2–4] Thus, researchers' attention has been focused on using a pure or doped polymer layer to enhance these devices' electric and dielectric properties, particularly in the last 20 years.[5–9] Polymers and their composites are advantageous due to their inexpensive, low weight per molecule, flexibility, suitable mechanical strength, ease of processing, appropriate dielectric strength, lightweight, and supreme capacity.[6,10,11] The synthesis of polymers with long chains results in thin films that are treated specifically in ways like cost effective, excellent strength, simple processing, and easy growth.[12] The use of metallic/metallic-oxide dopants at a percentage of 3–7% is able to easily improve the lower conductivity and dielectric values of pure polymers.[11,12]

PVC, or polyvinyl chloride, is a thermoplastic polymer with important insulating qualities. PVC's significant polarity makes it less effective as an electrical insulator than non-polar polymers. Mechanically speaking, PVC comes in two varieties: stiff and flexible, with corresponding elastic moduli of 1.5–15 MPa and 1500–3000 MPa. PVC has a melting point of 100 °C, however with the addition of a heat stabilizer, it may reach 260 °C. PVC has high values of dielectric loss tangent, volume resistivity, and dielectric constant, which make it suitable for use in the production of low-voltage and frequency insulation materials.[13] Physically speaking, Sm_2O_3 nanoparticles are seen as a powder that is pale yellow in color. Its molar mass and density are 351.82 g mol^{-1} and 8.43 g cm^{-3}, respectively. Samarium oxide nanoparticles have melting and boiling temperatures of 2335 and 4118 °C, respectively, at the thermal level. Samarium's electronic configuration is (Xe) $4f^6\ 6s^2$, whereas oxygen's configuration is (He) $2s^2\ 2p^4$. Furthermore, the chemical formula for samarium oxide, or Sm_2O_3, is composed of 13.75% O_2 and 86.23% Sm. It may be used to create a wide range of optoelectronic and microelectronic equipment, as well as gas sensors and capacitors.[14]

The electrical response of Schottky diodes (SDs) is dependent on the operating environment and influences their application in electronics technology. Additionally, because a sensitive lab is required, determining the electrical characteristics of SDs is a time-consuming and costly process. Consequently, high-reliability engineering methodologies that can predict the electrical features of SDs are required. Nevertheless, there are often large deviations from the ideal situation from the theoretical and empirically observed electrical properties using thermionic emission theory. Therefore, it makes sense to employ alternative methods that can reduce the quantity of experiments carried out, thereby conserving resources like time and money. At the moment, the most widely used method for accomplishing this objective is machine learning (ML). Research has proven that machine learning (ML) is applicable in most scientific and technical fields and has been effective in the field of Schottky configurations and the prediction of numerous electrical properties of them. Machine learning (ML) is a branch of artificial intelligence that may grow a simulation program to anticipate new data by analyzing data samples and creating rules and patterns.[15,16]

Machine learning (ML) is a powerful, highly accurate prediction tool that is used in many sectors and removes the need for human judgments and manipulations. A wide range of modeling methods are used in ML to train the regulations and subsequently anticipate new data. The ML approach has been used recently in the literature to analyze the electrical properties of SDs.[17,18]

To find out if these interfacial layers enhance the performance of MS structure, three different Au/n-Si (MS), Au/PVC/n-Si (MPS1), and Au/PVC: Sm_2O_3/n-Si (MPS2) structures are conducted on the same n-Si wafer under the same circumstances. An overview of the procedures followed in order to prepare the Sm_2O_3 nanoparticles and make the SDs is given. First, the structural properties of the produced Sm_2O_3 are ascertained by employing field emission-scanning electron microscopy (FE-SEM) pictures. Second, based on the I–V measurements, several fundamental electronic parameters of the manufactured MS, MPS1, and MPS2 structures are computed and compared, i.e., I_0, n, Φ_{B0}, R_s, R_{sh}, RR, and N_{ss}. They are also obtained by the electronic current predicted by the support vector regression (SVR) of the machine learning (ML) approach. Furthermore, the current conduction mechanisms (CCMs) at the forward and reverse bias regions of the prepared devices will be determined and predicted. Eventually, the effectiveness of the SVM technique will be been assessed for correctly predicting the electronic characteristics and their CCMs into fabricated SDs by comparing the expected and actual outcomes.

2. Experimental Section

Precursors $Sm(NO_3)_3.6H_2O$ and NaOH, obtained from Sigma-Aldrich and Merck in Germany, were utilized to make samarium-oxide. First, 20^{cc} of deionized water (DW) was used to dissolve 1.78 g of samarium-nitrate and 0.24 g of sodium hydroxide. The NaOH solution was then added dropwise to the samarium-nitrate solution to create a 0.2 M solution. The final solution was placed in an autoclave and heated to 180 °C for a whole day. The mixture was produced, dried at a temperature of 35 °C, and rinsed four times with ethanol. The supplied nano-powder was calcined for 1 h at 700 °C in a furnace. It should be mentioned that 10 mg of Sm_2O_3 nano-powder was evenly dispersed in 5 mL of the produced solution after 0.5 g of PVC powder had been dissolved in 99.5 mL of DW to create the PVC: Sm_2O_3 composite interlayer. **Figure 1** shows the preparation steps of the Sm_2O_3 nanoparticles schematically.

On a single n-Si wafer (doped with Boron), the Au/n-Si (MS), Au/PVC/n-Si, (MPS1), and Au/PVC:Sm_2O_3/n-Si (MPS2) structures were executed. The wafer had dimensions of 5.08 cm in diameter, 300 μm in thickness, 1–10 Ω.cm resistivity, one-side polished, and (100) float-zone. Prior to manufacture, n-Si wafers were first cleaned in DW with 18 MΩ resistivity in an ultrasonic bath for ≈10 min. This was done to remove the native oxide layer on both sides of the wafers. Following that, it was washed for 3 min in acetone, hydrogen peroxide (H_2O_2), ammonium

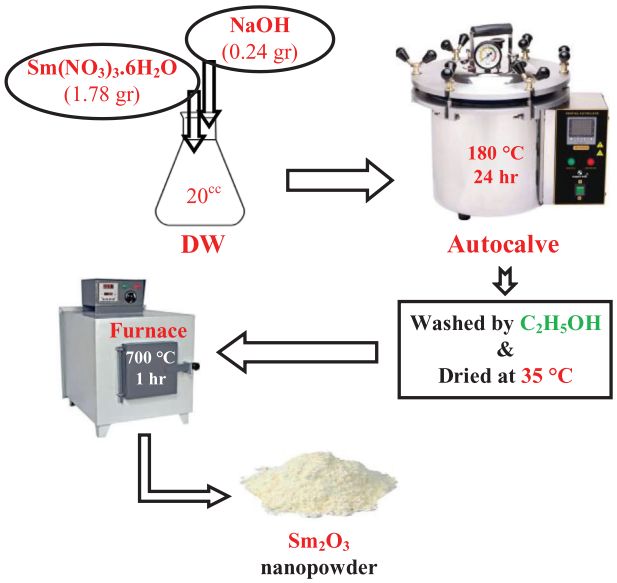

Figure 1. Steps of preparing Sm_2O_3 nanostructures.

hydroxide (NH_4OH), hydrofluoric acid (HF), and DW mixture/solution. The n-Si wafer was then dried using high-pure nitrogen gas (N_2) after being washed in the DW for 10 min. Second, after the n-Si wafer's surface was cleaned, 150 nm thick Au with a high purity of 99.999% was thermally evaporated onto the entire back side wafer in a high-vacuum metal-evaporation system at a rate of $\approx 10^{-6}$ Torr. To obtain good back-ohmic contact, the wafer was then annealed for 5 min at 550 °C in a N_2 atmosphere. In order to create the reference MS structure, one n-Si wafer was separated into three pieces. First, high-pure Au rectifier contacts with a circular shape, 7.85×10^{-3} cm^2 area and 150 nm thickness were grown onto one of the wafers. Consequently, MPS1 and MPS2 type structures were achieved under the same circumstances by thermally growing the similar-shaped, high-pure Au rectifier contacts onto the PVC and PVC: Sm_2O_3 composite interlayer. These three distinct samples are subjected to forward-reverse I–V measurements at ambient temperature using a KEITHLEY (Model 2450) apparatus.

Figure 2 schematically illustrates the energy-band diagrams for the manufactured MS, MPS1, and MPS2 structures.

2.1. SEM Analysis

The morphology of the produced Sm_2O_3 nanoparticles was examined using FE-SEM images that were obtained using the microwave technique. **Figure 3** shows the surface morphological patterns of the produced Sm_2O_3 nanoparticles as evaluated by the SEM with different scales. Although actual particle sizes were hard to observe, a variety of shaped, agglomerated, and polydispersity nanoparticles may be created. With a mean nanostructure size <1 μm, each nanoparticle is shown to have a unique form.

3. ML Approach

Machine learning is an important branch of artificial intelligence that is based in computer science, mathematics, statistics, and engineering. Its objective is to maximize the productivity of computer programmers by utilizing data and prior knowledge. Numerous related studies demonstrate the value of machine learning in rapidly extracting rules and patterns from available data, as it does so without requiring costly experiments or physical mechanisms. According to recent research, machine

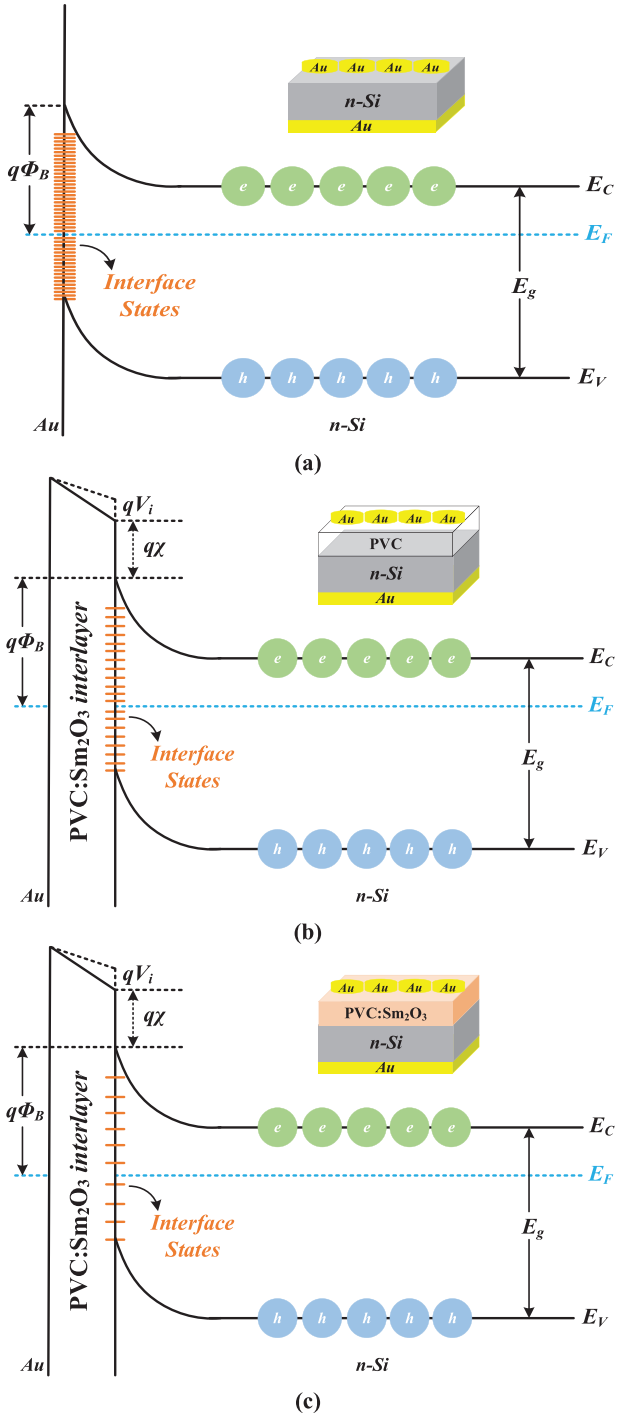

Figure 2. The energy-band diagram of the produced a) MS, b) MPS1, and c) MPS2 samples.

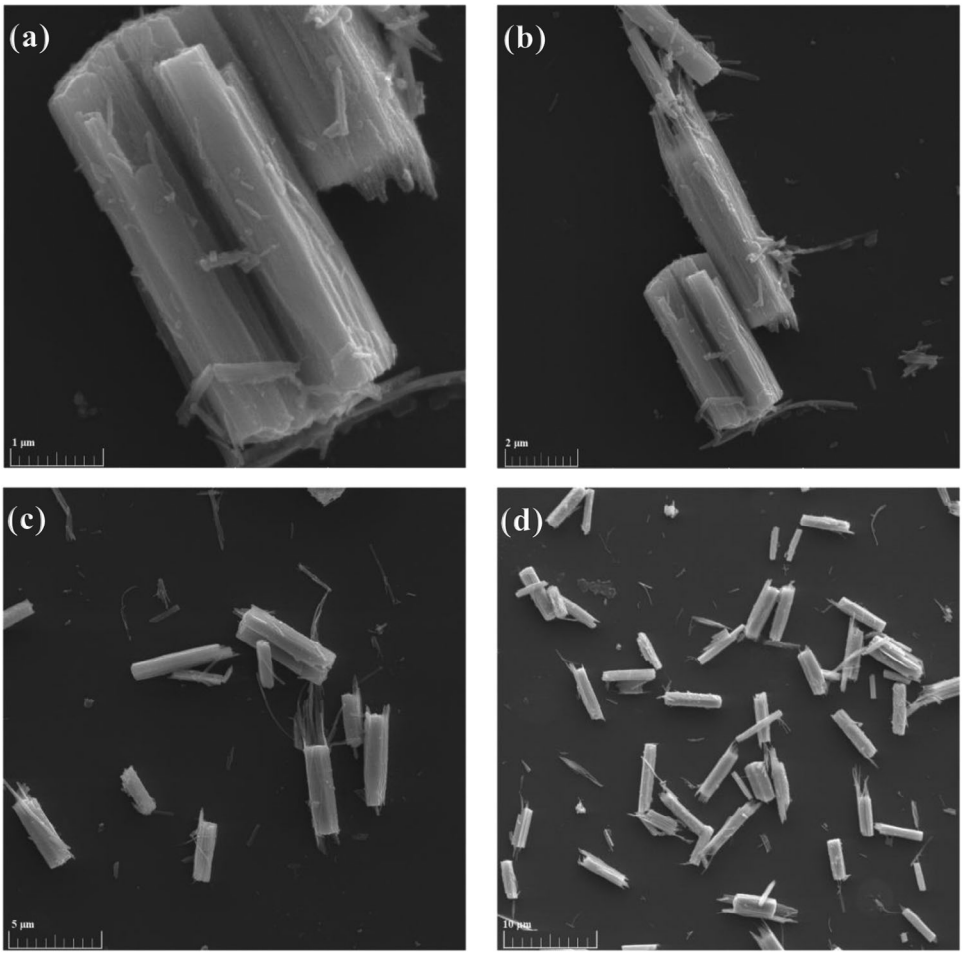

Figure 3. SEM picture of the synthesized Sm_2O_3 nanoparticles with different scales of a) 1, b) 2, c) 5, and d) 10 μm.

learning has been used to address many scientific and engineering difficulties, including those in computer vision, fundamental sciences (physics and chemistry), biology, health, technology, and even finance.[19–23] This work uses a machine learning approach, i.e., SVM, to model the I–V diagram and predict the CCMs into Schottky structures together with their different electronic features. Next, a comparison is made between the experimental data and the findings of the SVM algorithm. An overview of the SVM algorithm utilized in this work is introduced below.

3.1. SVR Model

Among the ML methods, Vapnik suggests is the Support Vector Method (SVM).[24] This approach uses a supervised learning model grounded on statistical methods to analyze pre-existing data for regression and classification analysis. The SVM training technique creates a model that decides which classification class each new data point belongs to, based on training data that has been labeled as belonging to one of two possible classes. To classify data, SVM maps them to a high-dimensional feature matrix. Naturally, data might not always be linearly separable. In any case, a hyperplane is applied to divide the classes and travels over as many data points as it can in a certain amount of time, or what is known as the margin.[25] As a result, by employing a kernel function, the SVR method can manage the non-linear relation between the input and target variables while reducing prediction error.

A training data set $T = \{(x_1, y_1), \ldots, (x_N, y_N)\}$ containing N ordered pairs of (x_i,y_i) for i = 1,2,...,N is considered. Here, x_i and y_i denote the features and their associated values, which are referred to as target values, respectively. In the SVR algorithm, a predicted value (y_p) for each feature (x_i) is deemed to be fitted with f(x). Therefore, the primary recommendation for implementing SVR is to develop a smooth regression profile f(x) with the least deviation value (ε) amidst the actual and target contents for all the data at the training data set. The SVR algorithm's estimate function, f(x), might be ascertained using:[26]

$$f(x) = w^T \varphi(x) + b \tag{1}$$

with b, $\varphi(x)$, and w being a constant, the feature function of input x, and the transposed weight vector, respectively. It is necessary

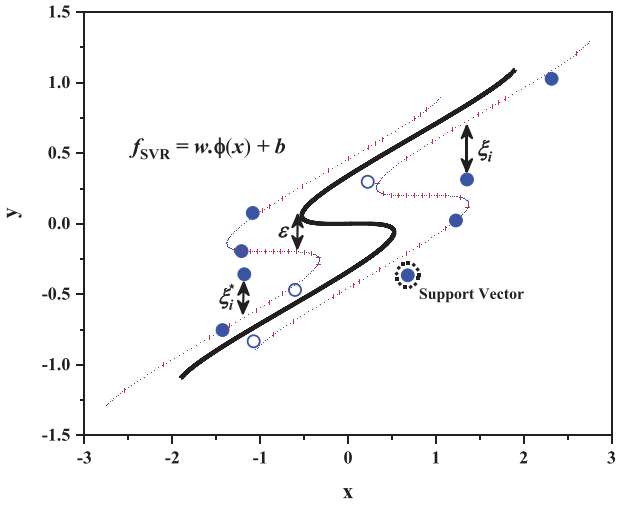

Figure 4. Schematic of SVR parameters.

to solve the convex optimization issue to have an appropriate regression function as:

$$\min \frac{1}{2}\|w\|^2 \; s.t. \; \begin{cases} y_i - w^T\varphi\left(x_i\right) - b \le \varepsilon \\ w^T\varphi\left(x_i\right) + b - y_i \le \varepsilon \end{cases} \tag{2}$$

It should be noted that there may not be a function f(x) that meets these requirements for every point. When the necessary criteria are satisfied, the positive and negative slack variables, ξ_i and ξ_i^*, can be supplied at each location to overcome the impractical limits:[26]

$$\min \frac{1}{2}\|w\|^2 + C\sum_{i=1}^{N}\left(\xi_i + \xi_i^*\right) \; s.t. \; \begin{cases} y_i - w^T\varphi\left(x_i\right) - b \le \varepsilon + \xi_i \\ w^T\varphi\left(x_i\right) + b - y_i \le \varepsilon + \xi_i^* \end{cases} \tag{3}$$

where C is a fixed penalty that helps avoid overfitting and $\xi_i, \xi_i^* \ge 0$ for all i by balancing the model complexity with the training set error. **Figure 4** shows the structural variables of the SVR model.

By transforming it into the dual problem at the Karush–Kuhn–Tucker (KKT) condition,[39] this optimization challenge may be resolved as:[26]

$$\max -\frac{1}{2}\sum_{i,j=1}^{N}\left(\beta_i - \beta_i^*\right)\left(\beta_j - \beta_j^*\right)\varphi(x_i)^T\varphi\left(x_j\right) - \varepsilon\sum_{i=1}^{N}\left(\beta_i + \beta_i^*\right) + \sum_{i=1}^{N} y_i\left(\beta_i - \beta_i^*\right) \; s.t. \left\{\sum_{i=1}^{N}\left(\beta_i - \beta_i^*\right) = 0 \right. \tag{4}$$

with $\beta_i, \beta_i^* \in [0, C]$ being the Lagrange multipliers. Once the dual problem has been resolved, the SVR function might then be indicated as follows:

$$f\ (x) = \sum_{i=1}^{N}\left(\beta_i - \beta_i^*\right)k\left(x_i, x_j\right) + b \tag{5}$$

here $k\left(x_i, x_j\right) = \varphi(x_i)^T\varphi(x_j)$ stands for the kernel function that is used to solve non-linear problems linearly.[27] It should be mentioned that the SVR algorithm is also implemented using the Radial Basis Function RBF.[25,26] Thus, it is provided by:

$$k\left(x_i, x_j\right) = exp\left(-\gamma\|x_i - x_j\|^2\right) \tag{6}$$

with γ being the kernel width. Each machine learning model is designed in three stages. The first step is to determine the hyperparameters that comprise the models. The SVR model design proceeds to the study of training and performance prediction. Finally, the verified model yields the predicted data. The effectiveness of the SVR method in predicting the electronic current of the SDs with various interfacial layers has been investigated.

3.2. Error and Accuracy Functions

As stated before, after the ML model construction is complete, a comprehensive analysis of prediction competency is needed. Furthermore, the computation and subsequent examination of the performance characteristics let us understand the prediction accuracy. Thus, in order to delineate the level of examination accuracy of the machine learning models employed in this work, the following functions representing mean absolute error (MAE) and mean squared error (MSE) were employed:[28]

$$MAE = \frac{1}{N}\sum_{i=1}^{N}\left|X_{\exp(i)} - X_{SVR(i)}\right| \tag{7}$$

$$MSE = \frac{1}{N}\sum_{i=1}^{N}\left(X_{\exp(i)} - X_{SVR(i)}\right)^2 \tag{8}$$

One of the extra measures that indicates the precision of the model is the R2 score. The model's training and hyperparameter selection inside the method is generally better when the R2 score is closer to one, producing predictions with a reduced mean square error (MSE). If the R2 score was zero, which would indicate that the hyperparameters were not chosen well, the model would perform badly on an unknown dataset. The model is deemed perfect if the R2 score value is one. The calculation is as follows:[26]

$$R2\ \text{Score} = 1 - \frac{\sum_{i=1}^{N}\left(X_{SVR(i)} - X_{\exp(i)}\right)^2}{\sum_{i=1}^{N}\left(\bar{X}_{\text{SVR}(i)} - X_{\exp(i)}\right)^2} \tag{9}$$

where X_{SVR}, X_{exp}, and $\bar{X}_{exp}$ represent, respectively, the mean amount of experiment data, the experiment value (actual value), and the anticipated value of the SVR model. When predicting the electronic current value of SDs in the absence or presence of various interlayers, **Figure 5** displays the MAE, MSE, and RMSE functions of the SVR approach that was considered. In the SVR model, it is clear that the MAE value for the MPS1 is smaller than the others when it comes to predicting the electronic current of the SDs under consideration. The MSE and RMSE figures for the provided SDs showed the same circumstance. **Figure 6** displays the R2 score of the SVR algorithm based on the hyperparameters C and γ in this ML technique. It is evident that when the values of C and γ in the SVR model increase, the R2 score for every sample increases as well. With $C = 10^5$ and $\gamma = 10^2$ being the optimal values for these hyperparameters, the R2 scores for MS, MPS1, and MPS2 SDs are 0.988, 0.996, 0.996, and 0.997, respectively.

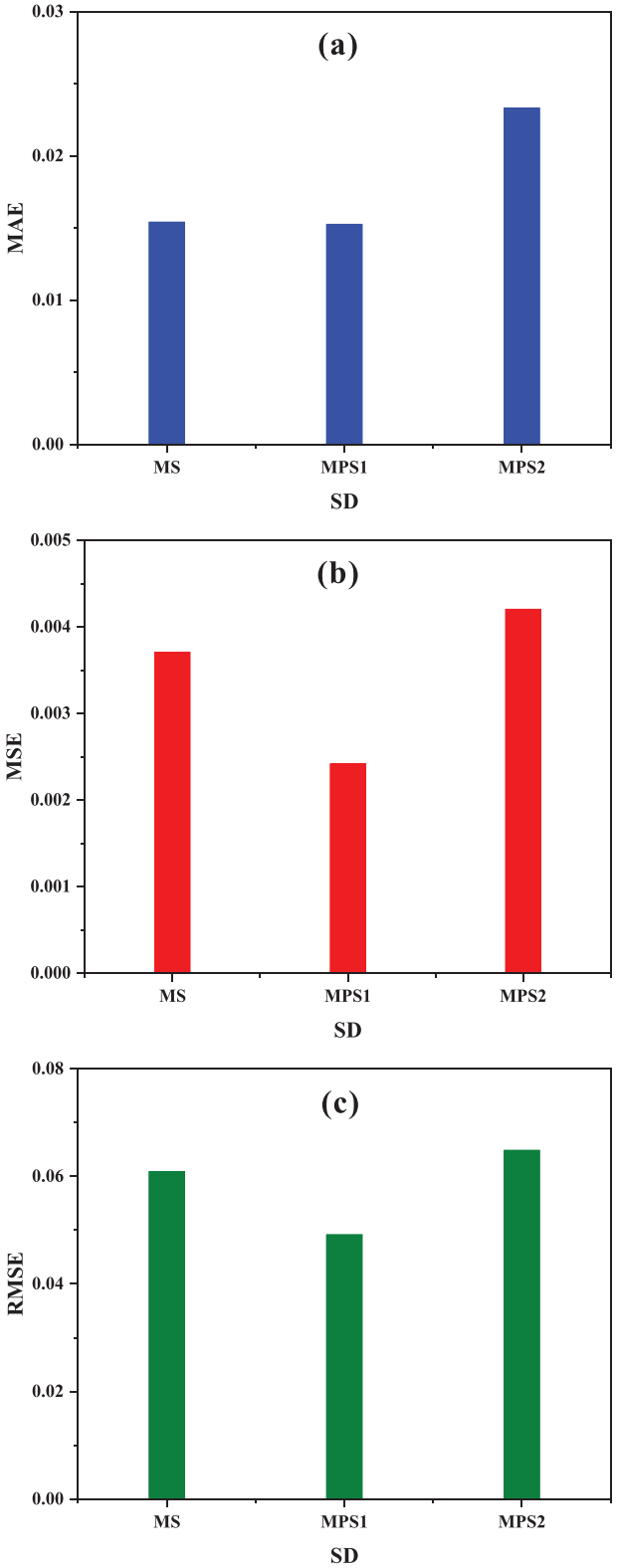

Figure 5. The a) MAE, b) MSE, and c) RMSE functions for the prediction of electronic current in the MS, MPS1, and MPS2 SDs by the SVR algorithm.

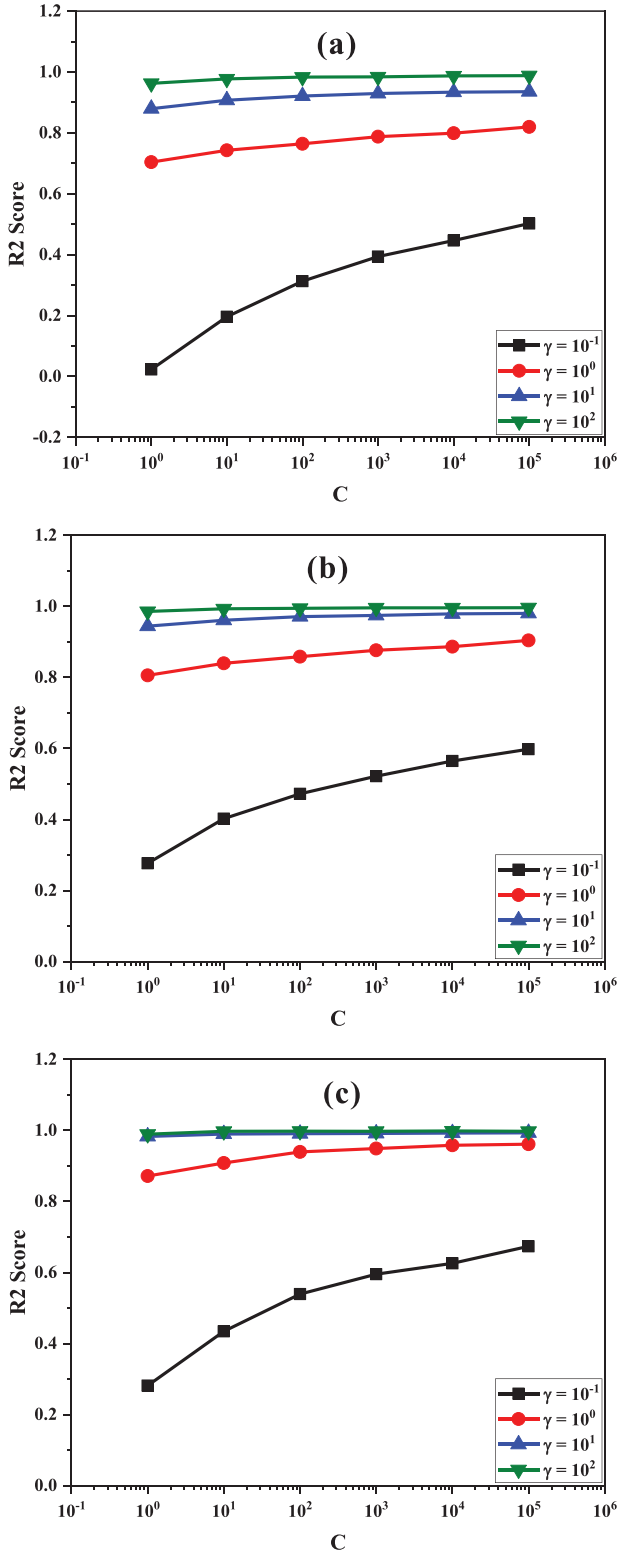

Figure 6. Dependence of the R2 score on the hyperparameters (C & γ) at the SVR algorithm for the a) MS, b) MPS1, and c) MPS2 SDs.

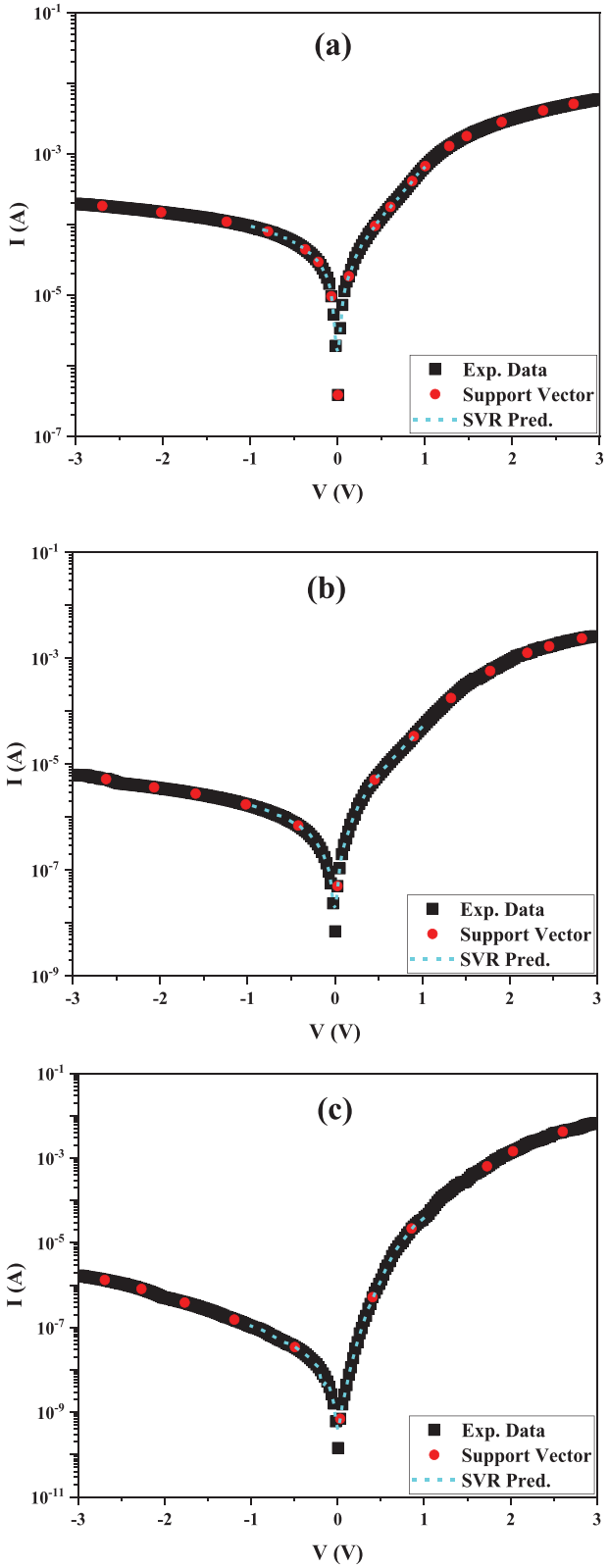

Figure 7. The experiment and predicted I–V characteristics of a) MS, b) MPS1, and c) MPS2 SDs.

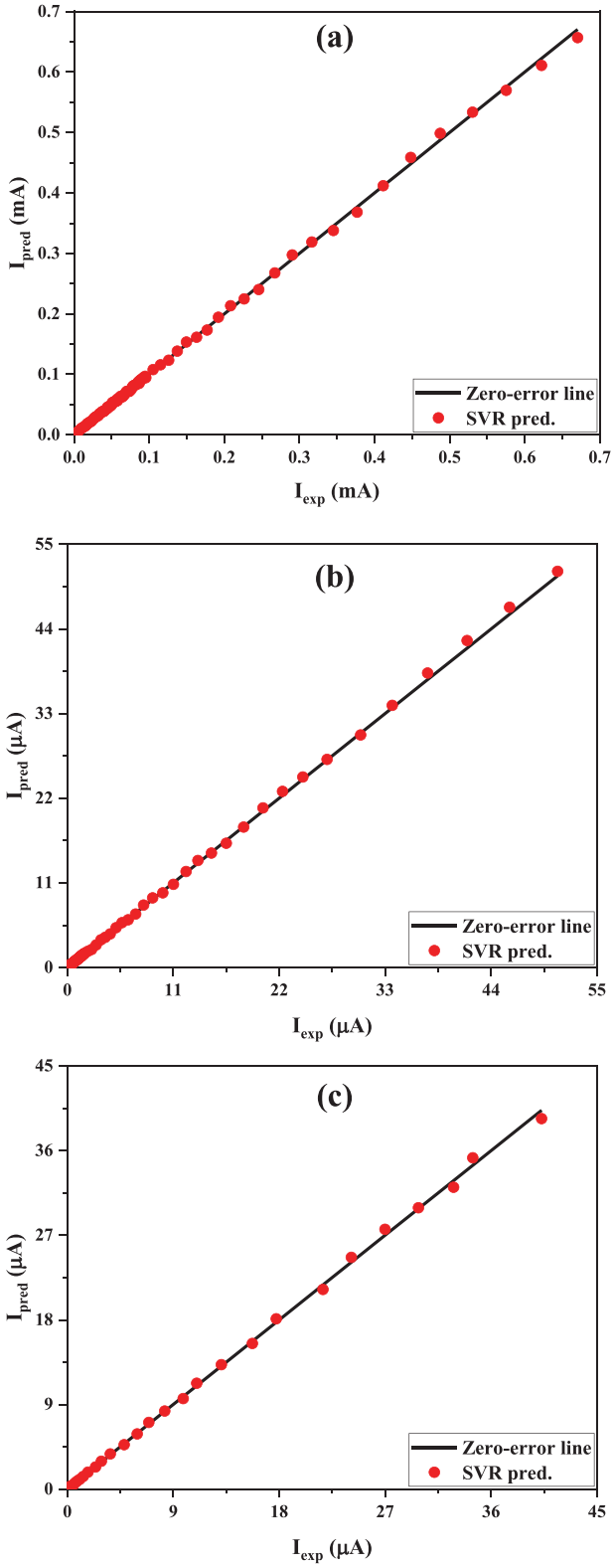

Figure 8. The prediction values of the SVR model for a) MS, b) MPS1, and c) MPS2 SDs.

Table 1. The actual and prediction quantities of I_0 for the fabricated SDs.

Val.	Actual						SVR					
SD	I_0 [nA]	Φ_{B0} [eV]	n	R_s [kΩ]	R_{sh} [MΩ]	RR	I_0 [nA]	Φ_{B0} [eV]	n	R_s [kΩ]	R_{sh} [MΩ]	RR
MS	7913	0.649	5.88	1.50	0.01	7	8000	0.648	5.92	1.53	0.01	6.9
MPS1	112	0.759	3.98	19.72	0.59	30	113	0.759	4.01	19.50	0.58	29
MPS2	0.82	0.887	2.28	24.92	9.26	372	0.81	0.887	2.26	25.48	9.09	357

4. Results and Discussion

Figure 7 semi-logarithmically depicts the I–V characteristic of the generated SDs in the absence or presence of pure PVC polymer and PVC:Sm_2O_3 composite interlayer using experimental data at ±3 V and SVR at ±1 V. Notably, the test size of 80 for the SVR algorithm was chosen to ensure predictions in the voltage range of −1 V to +1 V. Additionally, the TE theorem is used to analyze the I–V features of the provided SDs since, in contrast to previous techniques like Norde and Cheung, the ML methodology requires a very large quantity of data in order to predict the incoming data well. Remember that just electrons with sufficient energy to pass the barrier height of electric potential are taken into account for computing the current density, as the TE hypothesis depends on the BH having to be substantially bigger than kT. However, it is assumed that the emission-controlling plane has attained thermal equilibrium and that the equilibrium is unaffected by the presence of a net current flow.[29] Compared to the MS SD, the SVR model predicts the electronic current of the MPS SDs at different biases and confirms their error values (see Figure 4).

Figure 8 simultaneously displays the expected and real quantities for each SD without/with an interfacial layer of pure polymer and PVC:Sm_2O_3 composite to compare the prediction accuracy of the SVR model. The x- and y-axes, in that order, display the locations of the experiment and output data. Approximating data point placements is necessary to provide a more thorough grasp of prediction precision. In Figure 8, the zero-error line was specially created to aid in a closer examination of the positions of the data points. Another indication that the model is able to predict the electronic current with accuracy is the position of the SVR algorithm's data points with respect to the zero-error line.

According to the TE theorem, the I–V relationship in an SD might be provided for voltages in the forward bias area, assuming a R_s and voltages larger than 3kT q^{-1};[30]

$$I = I_0 \left[\exp\left(\frac{q\left(V - IR_s\right)}{nkT} \right) - 1 \right] \tag{10}$$

where, in turn, T, q, and k represent the temperature, electronic charge, and the Boltzmann constant. By using the linear part of the ln(I)-V plot at an applied voltage of 0 V, the content of I_0 could be derived as:[31]

$$I_0 = AA^* T^2 \exp\left(-\frac{q\varphi_{B0}}{kT} \right) \tag{11}$$

whose variables have been clearly presented in the literature.[30,31] The actual and predicted contents of I_0 for the constructed SDs using the SVR approach are shown in **Table 1**. It is evident that the SVR model's predicted value of I_0 most closely resembles the actual value. The pure PVC polymer and PVC:Sm_2O_3 composite interlayers cause the leakage electrical current to remarkably decrease, from 7.91 μA for the MS to 113 nA for the MPS1 and 0.82 nA for the MPS2.

Furthermore, the primary function of a nanocomposite interlayer in the MS SD is to regulate and control the height of potential barriers. Thus, one of the crucial electrical characteristics of SDs that needs to be achieved at zero voltage is:[31]

$$\varphi_{B0} = \frac{kT}{q} \ln\left(\frac{AA^* T^2}{I_0} \right) \tag{12}$$

Table 1 lists the BHs of the different created SDs. Besides, the electronic current needed to determine the BH of the SDs has been predicted using the ML approach, i.e., SVR. In this case, there is a good agreement between the actual value and the SVR algorithm's predictions. Additionally, as soon as the pure PVC polymer and PVC:Sm_2O_3 composite interlayers are put at the interface of semiconductor and metal layers, the BH of the MS junction has notably raised.

The ideality factor, which determines an SD's behavior with respect to the ideality diode, is one of the important electronic characteristics of SDs that this study examines. Since there is a native/deposited interlayer between the M-S layers, such as a polymer, insulator, ferroelectric, and composite materials, its quantity should ideally be unity, but it usually deviates from the ideal conditions. The density of surface/interface states produced between the interlayer and semiconductor, the thickness of the depletion layer (defined by the concentration of donor/acceptor atomic elements doped into the semiconductor), the amount of dielectric, and the thickness of the interlayer are other significant factors in defining the ideality factor. The ideality factor is often indicated by the slope of the ln(I)-V profile as:[31,32]

$$n = \frac{q}{kT} \left(\frac{dV}{d\left(\ln I\right)} \right) \tag{13}$$

It is important to note that additional processes influencing the ideality factor and CCMs into the MPS structures include electron tunneling through the electric potential barrier with surface states, e^--h^+ pair formation and recombination, and barrier reduction as a result of image-force impact.[1,33] Table 1 presents the obtained value of n for the built SDs in absence or presence of pure PVC and PVC:Sm_2O_3 composite interlayers at the M/S interface. Its drop from 5.88 for MS to 3.98 for MPS1 and 2.28 for MPS2 indicates that the existence of the pure PVC and PVC:Sm_2O_3 composite interlayer brings the SD response closer

to the ideal scenario. Once again, the SVR algorithm has estimated the n value for the taken-into-account SDs. The SVR model has exceptional precision and minimal deviation when determining the ideality coefficient of synthetic SDs.

Series resistance is one electronic feature of diodes that affects the rectification ratio (RR) and, in turn, the performance of SDs (R_s). Some sources from which it originated are the probe wires; the ohmic and rectifying junctions deposited on the backside and foreside of the semiconductor layer; the resistance of the semiconductor; the donor/acceptor atomic elements doped non-uniformly in the pure semiconductor; and the residual contaminations from the cleaning process among the contacts.[34–36] Although the R_s may be ignored at the inversion and depletion zones, they will perform better in the accumulation zone.[1,2] In this study, the ohmic law is used to calculate the values of R_s and R_{sh} as follows:

$$R_i = \frac{dV_i}{dI_i} \tag{14}$$

Table 1 displays the quantity of R_s obtained for the constructed SDs in absence or presence of the pure PVC polymer and PVC:Sm_2O_3 composite interlayers at an applied voltage of +1 V. Furthermore, the series resistance value of the taken-into-account SDs is predicted using the SVR approach. As can be seen, there is a fair amount of agreement between the actual numbers and the predictions produced by the SVR algorithm.

The causes of the shunt resistance (R_{sh}) at the reverse bias voltage are phenomena such as contaminants at the contact area, probing wire-ground patches, and leakage current across the nanocomposite interlayer.[36] Moreover, the applied voltage (V_a) is shared throughout the MPS SD with R_s and N_{ss}, provided $V_a = V_i + V_{Rs} + V_d + V_{ss}$. For sufficiently large positive voltages, this results in a deviation of the ln(I)-V plot from the linearity formulation.[37] Table 1 presents the value of R_{sh} for the produced SDs in the absence or presence of the pure PVC polymer and PVC:Sm_2O_3 composite interlayers, measured at ambient temperature and a negative bias voltage of −1 V. The MS SD's shunt resistance is increased by ≈50 and 900 times using the pure PVC polymer and PVC:Sm_2O_3 composite interlayers, respectively. The content of R_{sh} has been computed using the SVR approach in order to compare with the real values. With the least amount of variance from the actual numbers, the SVR model has predicted the R_{sh} value. For the studied SDs, the SVR predictions of the R_{sh} quantities are the ones that are closest to the real values.

On the other hand, the RR factor, also known as the ratio of the current at an applied voltage in the forward to the reverse regions as $RR = I_F/I_R$, is another characteristic that gives the rectifying rate of the MS and MPS SDs.[37] The RR amount of the produced SDs used in this investigation at room temperature is shown in Table 1. It is shown that by putting the pure PVC polymer and PVC:Sm_2O_3 composite interlayers at the MS contact, the RR of the MS structure will be considerably improved by 4 and 53 times. The electronic currents predicted by the SVR at the reverse and forward biases may be utilized to calculate the RR contents of different SDs, as the SVR algorithm has predicted the electronic current of the produced SDs at a voltage range from −1 V to +1 V. The highest degree of agreement between the predicted and actual amounts can be observed in the RR contents (see Table 1).

Table 2. The actual and prediction quantities of Nss for the fabricated SDs.

N_{ss} [eV^1 cm^{-2}] SD	Actual	SVR
MS	4.03×10^{13}	4.01×10^{13}
MPS1	6.55×10^{12}	6.57×10^{12}
MPS2	6.68×10^{10}	6.71×10^{10}

It is important to indicate that the SD deviates from ideal behavior for two reasons: the non-uniform distribution of the dopants in the semiconductor and surface/interface states. To understand the relevance of this defect by considering the voltage-dependent voltage supplied at the equilibrium state, the following method might be used:[38–41]

$$N_{ss}(V) = \frac{1}{q}\left[\frac{\varepsilon_i}{\delta}(n(V) - 1) - \frac{\varepsilon_s}{W_D}\right] \tag{15}$$

where δ represents the thickness of the pure PVC polymer and PVC:Sm_2O_3 interlayers (≈100 nm) and W_D refers to the depletion layer width. Furthermore, the semiconductor and interlayer permittivity are indicated by ε_s and ε_i, respectively. It should be noted that the following expression represents the energy difference between the valance band and N_{ss} states of a p-type semiconductor:[42]

$$E_{ss} - E_v = q(\varphi_e - V) \tag{16}$$

It must be noted that the φ_e, φ_{B0}, and n(V) are related to each other by the following relation:[42]

$$\varphi_e - \varphi_{B0} = \left(1 - \frac{1}{n(V)}\right) V \tag{17}$$

The prepared SDs introduced in **Table 2** can have their N_{ss} values calculated using Equations (15)–(17). The density of interface states is decreased when there is a pure polymer or composite interlayer between the metal and semiconductor layers. This is a result of the semiconductor layer's surface becoming passivated due to the pure polymer or composite interlayer.[35] Note that the development of potential BH, a native/deposited interlayer between the M/S layers, their uniform distribution, and the density of surface/interface states (N_{ss}) are responsible for the current conduction/transport processes into the SDs.[39–43] Moreover, the N_{ss} content for the given SDs is predicted using the SVR approach. The SVR algorithm's predictions and the actual values for the MS and MPS SDs coincide rather well.

Furthermore, the impact of the interlayer's presence or absence on the free carrier electronic current is compared throughout the SDs, and the CCM in the SDs' forward and reverse bias areas is investigated. It should be mentioned that in order to estimate the electronic current at the various voltage regions for further analysis, the test data's voltage location may be altered. Because of different CCMs, the Ln(I_F)-Ln(V_F) plots of the samples which are divided into two regions for the MPS2 SD and three regions for the MS and MPS1 SDs, are studied to extract their slopes. Charge transmission may generally be optimized by using deep traps that form at the contact and affect the I–V

Table 3. The actual and predicted values of the slope of Ln(IF)-Ln(VF) graphs for different samples.

Slope SD		Actual	SVR
MS	Part 1	2.491	2.465
	Part 2	1.536	1.536
	Part 3	1.190	0.905
MPS1	Part 1	1.994	1.981
	Part 2	3.577	3.562
	Part 3	1.362	1.135
MPS2	Part 1	4.782	4.780
	Part 2	1.170	0.870

characteristics. **Table 3** introduces the slopes of the three different regions at the Ln(I_F)-Ln(V_F) profiles of the MS and SDs. Additionally, the slope amounts predicted by the SVR method are acquired (see Table 3).

The slight disparities between the actual and predicted values demonstrate how well the SVR model anticipates the CCMs into the fabricated SDs. Region I exhibits an ohmic behavior, or I–V, due to the slope's proximity to unity. The semiconductor is injected with little charge from the electrodes because of the low voltage in this component.[44] At region II, the electronic current varies exponentially, or I ≈ exp(cV), and the slope value is larger than two. Recombination-tunneling is the main CCM in this section.[45] However, the electronic current displays a power behavior (I–V^m) at region III, due to the dispersion of traps created by space-charge limited current (SCLC) at the band gap of the used Sm_2O_3 nanoparticles. If the injected electron concentration is greater than the equilibrium charge concentration, the SCLC transport process is triggered. It should be mentioned that during the SCLC process, increasing the number of electrons supplied from the electrode leads the space charge to rise and the traps to fill up.[46] As can be observed, the slopes predicted by the SVR algorithm are very close to the actual ones and hence, the SVR model is able to give the CCMs into the manufactured SDs at the forward bias region appropriately.

The slopes of the ln(I_R)-$V_R^{0.5}$ graphs should be obtained to look into the CCMs of MS and MPS SDs under reversed voltage bias. It should be noted that emissions mechanisms might be either Schottky or Poole–Frenkel (PF). The reverse electronic current (I_R) may be written as follows once the PFE mechanism is overcoming:[44,47]

$$I_R = I_0 \exp\left(\frac{\beta_{PF}}{kT}\sqrt{\frac{V}{d}}\right) \tag{18}$$

On the other hand, if the SE mechanism predominates, I_R is described as;

$$I_R = AA^*T^2 \exp\left(-\frac{\varphi_B}{kT}\right)\exp\left(\frac{\beta_{SE}}{kT}\sqrt{\frac{V}{d}}\right) \tag{19}$$

whose β_{SE} is the field lowering coefficient for the SE process, often two times of the β_{PF}. It is expressed as,[47,48]

$$\beta_{PF} = 2\,\beta_{SE} = \sqrt{\frac{q^3}{\pi\varepsilon_0\varepsilon_r}} \tag{20}$$

here ε_r denotes the dielectric permittivity of the interlayer. The variations of Ln(I_R) depending on $V_R^{0.5}$ for the MS and MPS SDs show the good linear parts whose slopes are applied for calculating β_{PF} coefficient. As a result, the field lowering coefficient value for MS and MPS SDs was calculated and shown in **Table 4**. Moreover, the SVR method employed in this work predicts the value of the β_{PF} coefficient for the MS and MPS SDs (see Table 4).

A comparison between the theoretical and experimental values of β_{PF} is necessary to calculate the CCM into the MS and MPS SDs under the voltages at reverse bias region. Table 4 presents the computed theoretical results of β_{PF} for the MS and MPS structures developed in this study. It is found that the SE mechanism for the MS structure and the PFE mechanism for the MPS SDs prevail at the negative bias area. The fact that the SVR model's predicted value of β_{PF} is quite similar to the actual values is important to notice since it shows that the SVR model can accurately anticipate the CCM into the MS and MPS structures at the negative bias region.

5. Conclusion

In this research, three SDs, Au/n-Si (MS), Au/PVC/n-Si (MPS1), and Au/PVC:Sm_2O_3/n-Si (MPS2), were constructed in order to study the impact of the pure PVC polymer and PVC:Sm_2O_3 composite interlayers on the fundamental electronic properties as well as the CCMs/CTMs of the MS SD. Subsequently, the principal electric factors of the SDs—I_0, Φ_{B0}, n, R_s, R_{sh}, RR, and N_{ss}—were computed and their CCMs at the forward/reverse bias were ascertained by measuring the I–V data and using the TE theorem. By the SVM approach, every previously mentioned electronic factor and the CCMs/CTMs have been predicted and compared with the experimental data.

The obtained results show that when the pure PVC polymer and PVC:Sm_2O_3 composite interlayers are used, the electronic variables of I_0, n, R_s, and N_{ss} for MS SD decrease, and the values of Φ_{B0}, R_{sh}, and RR increase. In addition, if the pure PVC and PVC:Sm_2O_3 inter layers lower the n value from 5.88 for MS to 3.98 for MPS1, and 2.28 for MPS2 the conduct of the MS configuration gets closer to the ideal state. The pure PVC polymer and PVC:Sm_2O_3 composite interlayers grow the RR value of the MS SD up to 4 and 53 times, respectively. Therefore, the rectification ration of the MS SD would be greatly improved by the

Table 4. The values of βPF for various structures are based on experimental, theoretical, and prediction data.

B_{PF} [eV^1 cm^{-2}] SD	Exp.	Theory	SVR
MS	3.267×10^{-6}	5.001×10^{-5}	2.387×10^{-6}
MPS1	2.097×10^{-5}	1.717×10^{-5}	2.097×10^{-5}
MPS2	4.490×10^{-5}	3.294×10^{-5}	4.507×10^{-5}

addition of a polymer or composite interlayer between the semiconductor and metal layers. Also, the PVC and PVC:Sm_2O_3 composite layers that deposits between the semiconductor and the metal causes the surface/interface state density of the MS structure to drop. As a result, the pure PVC polymer interlayer leads to improved performance of the MS SD, but it is doped by the Sm_2O_3 nanostructures greatly enhances the electronic features. It was discovered that distinct processes happened in the MS and MPS structures as a result of the ohmic, exponential, and power behaviors by obtaining the slopes of the various portions of the $Ln(I_F)$-$Ln(V_F)$ plots. The field-lowering coefficient of the prepared structures was measured at the reverse bias region. This revealed that the PFE process is the dominant CCM in the MPS structure due to the PVC and PVC:Sm_2O_3 layers being inserted between the metal and semiconductor layers, while the SE mechanism predominates in the MS configuration.

Moreover, the SVM algorithm is a good approach to predict the CCMs/CTMs occurring in the MS and MPS SDs at the forward/reverse bias regions, because the experiment and prediction values of the slopes at the positive bias voltage and the β_{PF} coefficient at the negative bias voltage are very close to each other. After training with 400 data points, the SVM model was also able to predict the basic electronic variables of the MS and MPS SDs. The electronic variable values—I_0, Φ_{B0}, n, R_s/R_{sh}, RR, and N_{ss}—of the prepared MS and MPS SDs were predicted by the SVM algorithm with high accuracy and minimal deviation from the actual results. The SVM model's predicting performance for the electronic current of SDs is reliable due to the MSE values. As a result, this study can provide valuable insights for future research initiatives that aim to identify alternative, more fitting algorithms and maximize their refinement and optimization.

Conflict of Interest

The authors declare no conflict of interest.

Author Contributions

Y.A.K. was responsible for methodology, supervision, project administration, and writing – review and editing. A.B. handled conceptualization, experiments, formal analysis, discussion, and writing – original draft. Y.B. contributed to supervision and writing – review and editing.

Data Availability Statement

The data that support the findings of this study are available from the corresponding author upon reasonable request.

Keywords

electronic properties, samarium oxide (Sm_2O_3) nanoparticles, schottky diode (SD), support vector machine (SVM)

Received: August 10, 2024
Published online:

[1] S. M. Sze, K. K. Ng, *Phys. Semicond. Devices* **2006**, *3*, 601.
[2] E. H. Nicollian, J. R. Brews, *Phys. Technol.* **1982**, *1*, 920.
[3] H. C. Card, E. H. Rhoderick, *J. Phys. D: Appl. Phys.* **1971**, *4*, 1589.
[4] R. T. Tung, *Appl. Phys. Rev.* **2014**, *1*, 011304.
[5] Y. Azizian-Kalandaragh, *Optoelectron. Adv. Mater. Rapid Commun.* **2010**, *4*, 174.
[6] Ş. Altındal, A. Barkhordari, Y. Azizian-Kalandaragh, B. S. Çevrimli, H. R. Mashayekhi, *Mater. Sci. Semicond. Process.* **2022**, *147*, 106754.
[7] M. H. Al-Dharob, H. E. Lapa, A. Kökce, A. F. Özdemir, D. A. Aldemir, Ş. Altındal, *Mater. Sci. Semicond. Process.* **2018**, *85*, 98.
[8] Y. Azizian-Kalandaragh, *J. Semicond. Technol. Sci.* **2018**, *18*, 91.
[9] O. Çiçek, Ş. Altındal, Y. Azizian-Kalandaragh, *IEEE Sens. J.* **2020**, *20*, 14081.
[10] V. R. Reddy, C. V. Prasad, *Mater. Sci. Eng., B.* **2018**, *231*, 74.
[11] G. Ersöz, İ. Yücedağ, Y. Azizian-Kalandaragh, I. Orak, Ş. Altındal, *IEEE Trans. Electron Devices* **2016**, *63*, 2948.
[12] P. F. Rocha, M. Zeghouane, S. Boubenia, F. Bassani, L. Vauche, E. Martinez, W. Vandendaele, M. Veillerot, B. Salem, *Adv. Electron. Mater.* **2024**, *10*, 2300528.
[13] R. Shokrani-Havigh, Y. A. Azizian-Kalandaragh, *J. Optoelectron. Adv. Mater.* **2017**, *19*, 283.
[14] D. Richard, L. A. Errico, M. Rentería, *Comput. Condens. Matter* **2018**, *16*, e00327.
[15] E. H. Houssein, Z. Abohashima, M. Elhoseny, W. M. Mohamed, *Expert Systems Appl.* **2022**, *194*, 116512.
[16] Y. Torun, H. Doğan, *Superlattices Microstruct.* **2021**, *160*, 107062.
[17] H. A. Ali, E. F. El-Zaidia, R. A. Mohamed, *Chin. J. Phys.* **2020**, *67*, 602.
[18] T. Güzel, A. B. Çolak, *Superlattices Microstruct.* **2021**, *153*, 106864.
[19] K. Crampon, A. Giorkallos, M. Deldossi, S. Baud, L. A. Steffenel, *Drug Discovery Today* **2022**, *27*, 151.
[20] B. Mueller, T. Kinoshita, A. Peebles, M. A. Graber, S. Lee, *Acute Med. Surg.* **2022**, *9*, e740.
[21] O. Ivanciuc, *Rev. Comput. Chem.* **2007**, *23*, 291.
[22] H. Doğan, S. Duman, Y. Torun, S. Akkoyun, S. Doğan, U. Atici, *Mater. Sci. Semicond. Process.* **2022**, *149*, 106854.
[23] T. Güzel, A. B. Çolak, *Mater. Today Commun.* **2022**, *33*, 104175.
[24] V. Vapnik, Statistical Learning Theory, **1998**, 1780.
[25] C. W. Hsu, C. C. Chang, C. J. Lin, A Practical Guide to Support Vector Classification, Department of Computer Science, National Taiwan University, **2003**.
[26] M. Awad, R. Khanna, *Efficient Learning Machines: Theories, Concepts, and Applications for Engineers and System Designers*, Springer Nature, New York **2015**.
[27] A. Ali, A. Abdulrahman, S. Garg, K. Maqsood, G. Murshid, *Greenhouse Gases: Sci. Technol.* **2019**, *9*, 67.
[28] E. Ahmadloo, S. Azizi, *Int. Commun. Heat Mass Transfer* **2016**, *74*, 69.
[29] K. Potje-Kamloth, *Crit. Rev. Anal. Chem.* **2002**, *32*, 121.
[30] Z. Durmus, A. Durmus, H. Kavas, *J. Mater. Sci.* **2015**, *50*, 1201.
[31] A. Barkhordari, A. Ş, G. Pirgholi-Givi, H. Mashayekhi, S. Özçelik, Y. Azizian-Kalandaragh, *Silicon* **2022**, *15*, 855.
[32] O. Vargas, Á. Caballero, J. Morales, *Electrochim. Acta* **2014**, *130*, 551.
[33] Ş. Altındal, A. Barkhordari, S. Özçelik, G. Pirgholi-Givi, H. R. Mashayekhi, Y. Azizian-Kalandaragh, *Phys. Scr.* **2021**, *96*, 125838.
[34] S. Kolahi, S. Farjami-Shayesteh, Y. Azizian-Kalandaragh, *Mater. Sci. Semicond. Process.* **2011**, *14*, 294.
[35] A. Barkhordari, S. Özçelik, Ş. Altındal, G. Pirgholi-Givi, H. Mashayekhi, Y. Azizian-Kalandaragh, *Phys. Scr.* **2021**, *96*, 085805.
[36] J. Ansaree, S. Upadhyay, *Process. Appl. Ceram.* **2015**, *9*, 181.
[37] P. Yu, B. Cui, Q. Shi, *Mater. Sci. Eng., A.* **2008**, *473*, 34.
[38] Ş. Altındal, A. Barkhordari, G. Pirgholi-Givi, M. Ulusoy, H. Mashayekhi, S. Özçelik, Y. Azizian-Kalandaragh, *Phys. Scr.* **2021**, *96*, 125881.

[39] N. Rahman, M. Husain, J. Yang, M. Sajjad, G. Murtaza, M. Ul Haq, A. Habib, A. Rauf, A. Karim, M. Nisar, M. Yaqoob, *Eur. Phys. J. Plus* **2021**, *136*, 347.
[40] M. Husain, N. Rahman, R. Khan, S. Zulfiqar, S. A. Khattak, S. N. Khan, M. Sohail, A. Iqbal, A. H. Reshak, A. Khan, *Int. J. Energy Res.* **2022**, *46*, 2446.
[41] M. Husain, N. Rahman, R. Khan, M. Sohail, A. A. Khan, H. O. Elansary, T. K. El-Abedin, E. A. Mahmoud, S. A. Abdelmohsen, A. Khan, *Semicond. Sci. Technol.* **2022**, *37*, 075004.
[42] J. Saddique, M. Husain, N. Rahman, R. Khan, A. Iqbal, M. Sohail, S. A. Khattak, S. N. Khan, A. A. Khan, A. H. Reshak, A. Khan, *Mater. Sci. Semicond. Process.* **2022**, *139*, 106345.
[43] M. Husain, N. Rahman, H. Albalawi, S. Ezzine, M. Amami, T. Zaman, A. U. Rehman, M. Sohail, R. Khan, A. A. Khan, A. Khan, *RSC Adv.* **2022**, *12*, 32338.
[44] M. Gökçen, T. Tunç, Ş. Altındal, I. Uslu, *Mater. Sci. Eng., B.* **2012**, *177*, 416.
[45] A. Tatarŏlu, A. A. Hendi, R. H. Alorainy, F. Yakuphanŏlu, *Chin. Phys. B.* **2014**, *23*, 057504.
[46] A. Buyukbas-Uluşan, S. A. Yerişkin, A. D. Tataroğlu, M. Balbaşı, Y. A. Kalandaragh, *J. Mater. Sci.: Mater. Electron.* **2018**, *29*, 8234.
[47] V. R. Reddy, V. Manjunath, V. Janardhanam, Y. H. Kil, C. J. Choi, *J. Electron. Mater.* **2014**, *43*, 3499.
[48] H. Schroeder, *J. Appl. Phys.* **2015**, *117*, 215103.